Operation of BaSi2 homojunction solar cells on p+-Si(111) substrates and the effect of structure parameters on their performance

著者（英）	Komomo Kodama, Yudai Yamashita, Kaoru TOKO, Takashi SUEMASU
journal or publication title	Applied physics express
volume	12
number	4
page range	041005
year	2019-04
権利	(C) 2019 The Japan Society of Applied Physics
URL	http://hdl.handle.net/2241/00155620

doi: 10.7567/1882-0786/ab0c4f

Operation of $BaSi_2$ homojunction solar cells on p^+-Si(111) substrates and the effect of structure parameters on their performance

Komomo Kodama[a], Yudai Yamashita[a], Kaoru Toko[a], and Takashi Suemasu[a*]

[a]*Institute of Applied Physics, Graduate School of Pure and Applied Sciences, University of Tsukuba, Tsukuba, Ibaraki 305-8573, Japan*

Operation of n^+-$BaSi_2$/p-$BaSi_2$(500 nm)/p^+-$BaSi_2$ homojunction solar cells on p^+-Si(111) is demonstrated, showing a saturation current density of 9.4 mA/cm^2 and an open-circuit voltage of 0.11 V under AM1.5 illumination. Photogenerated electrons deep in the p-$BaSi_2$ light absorber layer are likely to be transferred to the p^+-Si side, leading to negative values of internal quantum efficiency (*IQE*) at longer wavelengths. The negative *IQE* can be solved by extending the width of depletion region in the p-$BaSi_2$ light absorber layer by decreasing its hole concentration. The importance of Si substrate surface morphology is also discussed.

* Corresponding author at:

Institute of Applied Physics, Faculty of Pure and Applied Sciences, University of Tsukuba, Tsukuba, Ibaraki 305-8573, Japan

Electronic mail: suemasu@bk.tsukuba.ac.jp

At present, 90% of the solar cells in the market are based on crystalline silicon (c-Si), and the conversion efficiency (η) of c-Si solar cells has exceeded 26%.[1] η is now approaching the theoretical Shockley-Queisser limit,[2] determined by a narrow bandgap of 1.1 eV. Therefore, alternative wider-bandgap materials such as III-V semiconductors, chalcopyrites, CdTe, and perovskites are being examined.[3-7] Under such circumstances, we have paid special attention to barium disilicide ($BaSi_2$).[8-10] It is composed of earth-abundant Ba and Si, and has attractive features such as a suitable bandgap of 1.3 eV, a large absorption coefficient (α) of 3×10^4 cm^{-1} at 1.5 eV,[11-14] and a large bulk minority-carrier lifetime of 14 μs.[15] Furthermore, $BaSi_2$ epitaxial films can be grown on Si substrates,[16,17] and its bandgap can be increased by adding isoelectric elements like Sr and C.[18,19] $BaSi_2$ is therefore a material of choice for targeting η beyond 30% in a Si-based tandem solar cell. As a first step, we have achieved η approaching 10% in B-doped p-$BaSi_2$/n-Si heterojunction solar cells.[20-22] In a p-$BaSi_2$/n-Si solar cell, the built-in potential is as small as 0.2 V due to the low electron affinity of $BaSi_2$ (3.2 eV).[23] The experimentally obtained open-circuit voltage (V_{OC}) was therefore smaller than 0.5 V.[20-22] Hence, it is not easy to make a drastic improvement in the η of p-$BaSi_2$/n-Si solar cells. Therefore, we next moved on to $BaSi_2$ homojunction solar cells, and very recently demonstrated the photogenerated carrier separation by the built-in electric field in these diodes on p^+-Si(111).[24] However, we face two problems, that is, a small saturation current density (J_{SC}) of 1.3 mA/cm^2, and large leakage current.[24] Such a small J_{SC} was caused by zero or even negative internal quantum efficiency (*IQE*) at longer wavelengths around 800–1000 nm. Long wavelength light is absorbed in the deep region of the $BaSi_2$ light absorber layer. Thus, we need to improve the collection of these photogenerated carriers. The large leakage current was caused by defects around the p^+-$BaSi_2$/p^+-Si heterointerface.[25] A p^+-$BaSi_2$/p^+-Si junction is necessary to transfer holes into a p-Si substrate because there is a large valence-band offset (0.65 eV) at the heterointerface.[23] Prior to the growth of $BaSi_2$ layers by molecular beam epitaxy (MBE), the

protective oxide layer on the surface has to be removed by heating the substrate at 900 °C for 30 min in an ultrahigh-vacuum chamber. This process is called thermal cleaning (TC). Upon this TC, step bunching occurs to a far greater extent especially in the case of a low-resistivity (ρ) Si(111) substrate.[25] Step bunching causes the generation of defects around the p^+-$BaSi_2$/p^+-Si heterointerface, and thus degrades the pn junction, leading to the decrease in shunt resistance R_{SH} as discussed later. We therefore need to prevent this problem, too.

In this article, we aim to find solutions to the above two problems, and therefore put emphasis on the following points. First, we extended the depletion region width in a p-$BaSi_2$ light absorber layer so that it would be almost fully depleted. This is to efficiently collect the carriers photogenerated in the deep region of the p-$BaSi_2$ absorber layer by the built-in electric field. Second, we employed medium-doped p-Si(111) substrates (ρ = 1–4 Ωcm) rather than p^+-Si(111) substrates to prevent the step bunching upon heating the Si substrates for removing oxides. Heavily p^+-Si layers for a p^+-$BaSi_2$/p^+-Si junction were formed on the surface by implantation of B atoms. As a result, we succeeded to extend the long-wavelength edge of the *IQE* spectrum from 800 to 950 nm, corresponding to the band gap of $BaSi_2$, and achieved the first demonstration of distinct η in a $BaSi_2$ homojunction solar cell. The V_{OC} of 0.11 V, J_{SC} = 9.4 mA/cm^2, and η = 0.28% was obtained.

We used an ion-pumped MBE system equipped with an electron-beam evaporation source for 10N-Si as well as standard Knudsen cells for 3N-B, 5N-Sb, and 3N-Ba. Details of the growth procedure of undoped $BaSi_2$, Sb-doped n-$BaSi_2$, and B-doped p-$BaSi_2$ layers were reported previously.[20,26,27] Sample structures are summarized in Table I. We used low-ρ n^+-Si(111) substrates (ρ < 0.01 Ωcm) for sample A and p^+-Si(111) substrates (ρ < 0.01 Ωcm) for samples B-E. For sample F, B atoms were implanted into medium-doped p-Si(111) substrates (ρ = 1–4 Ωcm) with a dose of 2.5 × 10^{14} cm^{-2} and a projected range of 50 nm so that the hole concentration (p) would be approximately 2 × 10^{19} cm^{-3} on the surface after activation annealing

at 900 °C for 3 min. Sample G is a reference to compare the solar cell performance. Samples A-F were fabricated for the following reasons. We formed sample A to confirm the long-wavelength edge where the photoresponsivity sharply arises. For this purpose, we formed a 500 nm-thick undoped $BaSi_2$ epitaxial layer by MBE. Then, a 3 nm-thick amorphous Si (a-Si) capping layer was deposited *in situ* at 180 °C to prevent surface oxidation.[28] Finally, 80 nm-thick indium-tin-oxide (ITO) electrode with 1 mm diameter was sputtered on the front side and 150-nm-thick Al electrode was sputtered on the back side. In all the samples, a-Si capping layers and electrodes were formed under the same condition as sample A. In samples B-D, we formed three types of $BaSi_2$-pn homojunction diodes, n^+-$BaSi_2$(20 or 150 nm)/p-$BaSi_2$(500 nm)/p^+-$BaSi_2$(20 or 50 nm) on p^+-Si(111) substrate ($\rho < 0.01$ Ωcm) to compare their *IQE* spectra. The *p* of a 500 nm-thick B-doped p-$BaSi_2$ absorber layer was set at approximately 10^{17} cm^{-3}. In samples B and C, we investigated the effect of p^+-$BaSi_2$ layer thickness on the solar cell performance. This is because p^+-$BaSi_2$ layers often degrade the crystalline quality of p-$BaSi_2$ light absorber layers. In this respect, p^+-$BaSi_2$ should be as thin as possible. On the other hand, it was reported that p^+-$BaSi_2$ with a certain thickness is necessary to fully cover the p^+-Si substrate.[22] In sample D, the n^+-$BaSi_2$ layer was set at 150 nm so that photons with long wavelengths around 800 nm would be fully absorbed in the p-$BaSi_2$ light absorber layer. In samples E and F, we employed undoped p-$BaSi_2$ layers with p~10^{16} cm^{-3} instead of B-doped p-$BaSi_2$ layers,[29] and investigated the effect of depletion region width in the $BaSi_2$ light absorber layer as well as of the substrate surface morphology on the *IQE* spectra.

The current density versus voltage (*J*-*V*) characteristics under standard AM 1.5 illumination and photoresponse properties were measured. The photoresponse spectrum was measured using a xenon lamp with a 25-cm-focal-length single monochromator (Bunko Keiki SM-1700A and RU-60N). Reflectance spectra were evaluated with a reflection measurement system using a xenon lamp with an integrating sphere. All measurements were performed at

room temperature. The band alignments of samples C and E were simulated by automat for simulation of heterostructures (AFORS-HET), where the ideal condition such as no defects was assumed.[30]

Table I. Sample preparation details. Si substrate, thicknesses and designed carrier concentrations of p^+- $BaSi_2$, p-$BaSi_2$ light absorber, and n^+-$BaSi_2$ are given.

Sample	Si substrate	p^+-$BaSi_2$	p-$BaSi_2$ absorber	n^+-$BaSi_2$
A	n^+-Si(111), $\rho < 0.01$ Ωcm	–	Undoped, 500 nm $p \sim 10^{15}$ cm^{-3}	–
B	p^+-Si(111), $\rho < 0.01$ Ωcm	B-doped, 50 nm, $p \sim 10^{19}$ cm^{-3}	B-doped, 500 nm, $p \sim 10^{17}$ cm^{-3}	Sb-doped, 20 nm, $n \sim 10^{19}$ cm^{-3}
C	p^+-Si(111), $\rho < 0.01$ Ωcm	B-doped, 20 nm, $p \sim 10^{19}$ cm^{-3}	B-doped, 500 nm, $p \sim 10^{17}$ cm^{-3}	Sb-doped, 20 nm, $n \sim 10^{19}$ cm^{-3}
D	p^+-Si(111), $\rho < 0.01$ Ωcm	B-doped, 20 nm, $p \sim 10^{19}$ cm^{-3}	B-doped, 500 nm, $p \sim 10^{17}$ cm^{-3}	Sb-doped, 150 nm, $n \sim 10^{19}$ cm^{-3}
E	p^+-Si(111), $\rho < 0.01$ Ωcm	B-doped, 20 nm, $p \sim 10^{19}$ cm^{-3}	Undoped, 500 nm, $p \sim 10^{16}$ cm^{-3}	Sb-doped, 20 nm, $n \sim 10^{19}$ cm^{-3}
F	implanted p^+-Si/ p-Si(111), ρ = 1–4 Ωcm	B-doped, 20 nm, $p \sim 10^{19}$ cm^{-3}	Undoped, 500 nm, $p \sim 10^{16}$ cm^{-3}	Sb-doped, 20 nm, $n \sim 10^{19}$ cm^{-3}
G[21]	n-Si(111), ρ = 1–4 Ωcm	B-doped, 20 nm, $p \sim 10^{18}$ cm^{-3}	–	–

Figure 1(a) shows the photoresponse spectrum of sample A. A bias voltage (V_{bias}) of 1 V was applied to the front ITO electrode with respect to the back Al electrode to collect

photogenerated electrons to the ITO. V_{bias} was necessary to extract photogenerated carriers for sample A because there was no built-in electric field in sample A. The photoresponsivity appeared pronounced at wavelengths shorter than approximately 1000 nm, close to the band gap of $BaSi_2$. Figure 1(b) shows the *IQE* spectra of samples B–E for $BaSi_2$ homojunction solar cells, obtained at V_{bias} = 0 V, showing that the built-in electric field surely separated photogenerated carriers. Compared with the spectrum of sample A in Fig. 1(a), however, the *IQE* values at wavelengths between 800 and 1000 nm were negligibly small or even negative in samples B–D. This trend was pronounced in sample D. These results show that the photogenerated carriers deep in the p-$BaSi_2$ absorber layer are difficult to be extracted by the built-in electric field or are transferred in the opposite direction. Figure 1(c) shows the V_{bias} dependences of *IQE* spectra for sample D. With increasing V_{bias} from 0 to 0.2 V to extract photogenerated electrons to the ITO electrode, the *IQE* becomes positive in the whole wavelength region. In sample D, the total thickness of n^+-$BaSi_2$ and p-$BaSi_2$ layers is 650 nm. The value of α at a wavelength of 800 nm is around 3×10^4 cm^{-1}, meaning that the penetration depth at this wavelength is estimated to be $2/\alpha$ = 0.66 μm. Therefore, photons with this wavelength are fully absorbed in the 500 nm-thick p-$BaSi_2$ absorber layer. This is the reason why the negative *IQE* was distinct in sample C. We discuss this result by using the band alignment of sample C shown in Fig. 2(a). The bottom of the conduction band (E_C) of the neutral p-$BaSi_2$ region is positioned a little higher than that of p^+-Si. Therefore, the photogenerated electrons in the deep neutral p-$BaSi_2$ region are likely to be transferred to the p-Si side. We think that such flow of carriers is promoted because there is a number of defect levels at the p^+-$BaSi_2$/p^+-Si interface. On the other hand, in sample E, the long-wavelength edge of the *IQE* spectrum shifted from 800 to 850 nm in Fig. 1(b). We ascribed this shift to the decrease of *p* in the p-$BaSi_2$ absorber layer from approximately 10^{17} to 10^{16} cm^{-3}. Figure 2(b) shows the band alignment of sample E, where the width of depletion region increased by approximately 3 times

compared to that in sample C shown in Fig. 2(a). Please note that the absorber layer is almost fully depleted in sample E, and thereby the electric field might promote the separation of photogenerated carriers, resulting in the improved *IQE* in the long wavelength range. The *IQE* spectrum was further improved in sample F.

Figure 3(a) shows the *IQE* spectra of samples E and F. In sample F, the long-wavelength edge of the *IQE* spectrum further shifted from 850 to 950 nm, almost close to the band gap of $BaSi_2$. This result shows that the formation of p^+-Si surface layer by implanting B at a position slightly deeper from the surface is an effective means to extend the *IQE* spectrum toward the longer wavelength range. However, the *IQE* was decreased unexpectedly in the short wavelength range when we compared the *IQE* spectra of samples E and F in Fig. 3(a) with those of samples B–D in Fig. 1(a). This means that the collection of photogenerated carriers in the region close to the surface was degraded in samples E and F. The difference between them is that undoped p-$BaSi_2$ layers were adopted in samples E and F, whereas B-doped p-$BaSi_2$ layers were used in samples B–D. We speculate that the carrier type of the undoped $BaSi_2$ absorber layer in samples E and F would change from p-type to n-type in the region somewhere in the $BaSi_2$ light absorber layer, leading to the decrease in built-in electric field there, and thus degrading the *IQE* in the short wavelength range. This is because undoped p-$BaSi_2$ layers change to an n-type conductivity when the Ba to Si atomic ratio deviates from stoichiometry, and the supply of Si atoms from the Si substrate tends to be deficient as moving towards the surface of $BaSi_2$ layers.[26] Therefore, the formation of lightly-B doped p-$BaSi_2$ layers with $p \sim 10^{16}$ cm^{-3} is mandatory to improve the *IQE* spectrum, and this would be our key challenge.

The *J*-*V* curves under AM 1.5 illumination for samples B, E and F are shown in Fig. 3(b). V_{OC} and J_{SC} were improved significantly in samples E and F compared to sample B. Sample F showed $\eta = 0.28\%$, $J_{SC} = 9.42$ mA/cm^2, and $V_{OC} = 0.11$ V. To accurately determine the series resistance (R_S) and R_{SH} of a diode, we adopted a technique described by Sites and

Mauk,[31] and summarized in Table II.

Table II. Solar cell parameters of samples E, F, and G.[21]

Sample	J_{SC} [mA/cm^2]	V_{OC} [V]	R_S [Ω]	R_{SH} [Ω]	η [%]
E	4.3	0.034	149	1430	0.04
F	9.4	0.113	145	6954	0.28
G[21]	35.2	0.476	128	10046	9.9

R_{SH} differs significantly between samples E-G, whereas there is not so much difference in R_S. In sample E, the R_{SH} is the smallest, meaning that the leakage current is the highest. The R_{SH} increases in the order of samples E, F, and G. We attribute a small R_{SH} to defects around the p^+-$BaSi_2$/p^+-Si interface because surface morphology of a Si substrate before the growth of $BaSi_2$ layers affects the formation of defects significantly.[25] Figure 4 shows the atomic force microscopy (AFM) topographic views (2 × 2 μm^2) and cross-sectional profiles (along while lines) of the Si substrate surfaces of these samples taken after TC. The root-mean-square (RMS) surface roughness values and reflection high-energy electron diffraction (RHEED) patterns are also presented. The minimum step height of the Si(111) surface is 0.31 nm, and such a surface was obtained in Fig. 4(c) for sample G. The RHEED pattern was surely on the Laue ring, meaning the atomically flat surface. Similar RHEED pattern was obtained in Fig. 4(b) for sample F. On the other hand, in Fig. 4(a), streaky RHEED pattern was observed for sample E, showing the degradation of surface smoothness compared to sample F. Furthermore, the step edge on the surface was not straight but rather complex. We speculate that this kind of difference in surface morphology of the p^+-Si(111) surface prior to the growth of $BaSi_2$ films affects the defect formation around the p^+-$BaSi_2$/p^+-Si interface. Therefore, realization of a smooth p^+-Si(111) surface while ensuring a good electrical contact between p^+-$BaSi_2$/p^+-Si is

the key to increasing R_{SH}, and thereby achieving higher η.

In summary, we formed several kinds of $BaSi_2$ homojunction solar cells with a 500 nm-thick p-$BaSi_2$ light absorber layer. When the hole concentration of the p-$BaSi_2$ absorber layer was approximately 10^{17} cm^{-3}, the *IQE* was almost zero or negative at long wavelengths. This problem was improved drastically by decreasing the p down to 10^{16} cm^{-3}, and by using B implanted medium-doped p-Si(111) substrate. The long-wavelength edge of the *IQE* spectrum extended to around 950 nm, leading to the first demonstration of $BaSi_2$ solar cells with distinct η = 0.28%, V_{OC} = 0.11 V, and J_{SC} = 9.4 mA/cm^2.

Acknowledgements

This work was financially supported by JSPS KAKENHI Grant Numbers 17K18865 and 18H03767 and JST MIRAI.

References

[1] K. Yoshikawa, H. Kawasaki, W. Yoshida, K. Konishi, K. Nakao, T. Uto, D. Adachi, M. Kanematsu, H. Uzu, and K. Yamamoto, Nat. Energy **2**, 17032 (2017).

[2] W. Shockley, and H. J. Queisser, J. Appl. Phys. **32**, 510 (1961).

[3] P. Jackson, D. Hariskos, R. Wuerz, O. Kiowski, A. Bauer, T. M. Friedlmeier, and M. Powalla, Phys. Status Solidi RRL **9**, 28 (2015).

[4] P. Jackson, R. Wuerz, D. Hariskos, E. Lotter, W. Witte, and M. Powalla, Phys. Status Solidi RRL **10**, 583 (2016).

[5] X. Wu, Sol. Energy **77**, 803 (2004).

[6] J. Burschka, N. Pellet, Soo-Jin Moon, R. Humphry-Baker, P. Gao, M. K. Nazeeruddin, and M. Grätzel, Nature **499**, 316 (2013).

[7] W. S. Yang, J. H. Noh, N. J. Jeon, Y. C. Kim, S. Ryu, J. Seo, and S. I. Seok, Science **348**, 1234 (2015).

[8] T. Nakamura, T. Suemasu, K. Takakura, F. Hasegawa, A. Wakahara, and M. Imai, Appl. Phys. Lett. 81, 1032 (2002).

[9] T. Suemasu, Jpn. J. Appl. Phys., Part 1 **54**, 07JA01 (2015).

[10] T. Suemasu and N. Usami, J. Phys. D: Appl. Phys. **50**, 023001 (2017).

[11] K. Morita, Y. Inomata, and T. Suemasu, Thin Solid Films **508**, 363 (2006)

[12] D. B. Migas, V. L. Shaposhnikov, and V. E. Borisenko, Phys. Status Solidi (b) **244**, 2611 (2007).

[13] K. Toh, T. Saito, and T. Suemasu, Jpn. J. Appl. Phys. **50**, 068001 (2011).

[14] M. Kumar, N. Umezawa, and M. Imai, Appl. Phys. Express **7**, 071203 (2014).

[15] K. O. Hara, N. Usami, K. Nakamura, R. Takabe, M. Baba, K. Toko, and T. Suemasu, Appl. Phys. Express **6**, 112302 (2013).

[16] R. A. McKee, F. J. Walker, J. R. Conner, E. D. Specht, and D. E. Zelmon, Appl. Phys. Lett. 59, 782 (1991).

[17] R. A. McKee and F. J. Walker, Appl. Phys. Lett. 63, 2818 (1993).

[18] K. Morita, M. Kobayashi, and T. Suemasu, Jpn. J. Appl. Phys. **45**, L390 (2006).

[19] Y. Imai and A. Watanabe, Intermetallics **18**, 1432 (2010).

[20] D. Tsukahara, S. Yachi, H. Takeuchi, R. Takabe, W. Du, M. Baba, Y. Li, K. Toko, N. Usami, and T. Suemasu, Appl. Phys. Lett. **108**, 152101 (2016).

[21] S. Yachi, R. Takabe, H. Takeuchi, K. Toko, and T. Suemasu, Appl. Phys. Lett. **109**, 072103 (2016).

[22] T. Deng, T. Sato, Z. Xu, R. Takabe, S. Yachi, Y. Yamashita, K. Toko, and T. Suemasu, Appl. Phys. Express **11**, 062301 (2018).
[23] T. Suemasu, K. Morita, M. Kobayashi, M. Saida, and M. Sasaki, Jpn. J. Appl. Phys. **45**, L519 (2006).
[24] K. Kodama, R. Takabe, T. Deng, K. Toko, and T. Suemasu, Jpn. J. Appl. Phys. **57**, 050310 (2018).
[25] Y. Yamashita, S. Yachi, R. Takabe, T. Sato, M. Emha Bayu, K. Toko, and T. Suemasu, Jpn. J. Appl. Phys. **57**, 025501 (2018).
[26] R. Takabe, T. Deng, K. Komomo, Y. Yamashita, T. Sato, K. Toko, and T. Suemasu, J. Appl. Phys. **23**, 045703 (2018).
[27] K. Kodama, R. Takabe, S. Yachi, K. Toko, and T. suemasu, Jpn. J. Appl. Phys. **57**, 031202 (2018).
[28] R. Takabe, H, Takeuchi, W. Du, K. Ito, K. Toko, S. Ueda, A. Kimura, and T. Suemasu, J. Appl. Phys. **119**, 165304 (2016).
[29] Y. Yamashita, T. Sato, K. Toko, A. Uedono, and T. Suemasu, Ext. Abstr. (79th Autumn Meet., 2018), Japan Society of Applied Physics and Related Societies, 19p-436-15 [in Japanese].
[30] R. Varache, C. Leendertz, M. E. Gueunier-Farret, J. Haschke, D. Muñoz, and L. Korte, Sol. Energy Mater. Sol. Cells **141**, 14 (2015).
[31] J. R. Sites and P. H. Mauk, Sol. Cells **27**, 411 (1989).

Figure captions

Fig. 1. (a) Photoresponse spectrum of sample A, 500 nm-thick undoped $BaSi_2$ layer with R_{Ba}/R_{Si} ~ 2, measured under a bias voltage of 1 V applied to the front ITO electrode with respect to the back Al electrode. (b) *IQE* spectra of samples B–E.

Fig. 2. Calculated band alignments of $BaSi_2$ n^+-p-p^+ homojunction diodes on p^+-Si(111) by AFORS-HET for (a) sample C and (b) sample E. The *p* of the p-$BaSi_2$ absorber layer is approximately 10^{17} cm^{-3} in sample C and 10^{16} cm^{-3} in sample E. The arrows indicate the flow of photogenerated electrons.

Fig. 3. (a) *IQE* spectra of samples E and F and (b) *J-V* characteristics of samples B, E, and F under AM1.5 illumination.

Fig. 4. Topographic AFM views (2×2 μm^2) and cross-sectional profiles (along white lines) of the Si substrate surface taken after the thermal cleaning in UHV for samples (a) E, (b) F and (c) G. RMS surface roughness values and RHEED patterns are presented.

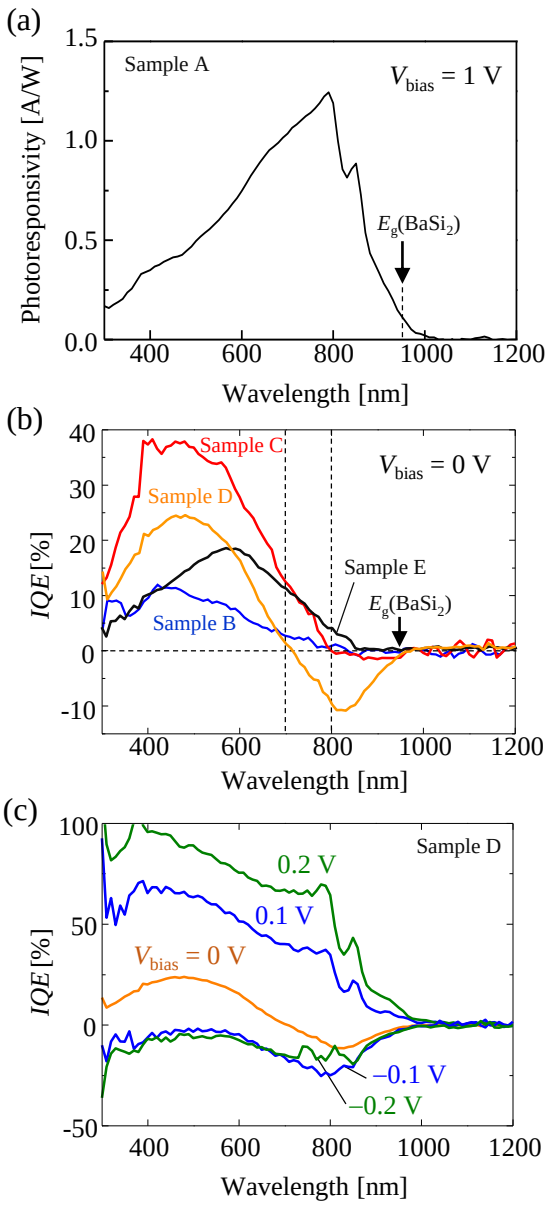
(a)
Sample A
V_{bias} = 1 V
E_g(BaSi$_2$)
Photoresponsivity [A/W]
Wavelength [nm]
(b)
Sample C
Sample D
Sample E
Sample B
V_{bias} = 0 V
E_g(BaSi$_2$)
IQE [%]
Wavelength [nm]
(c)
Sample D
0.2 V
0.1 V
V_{bias} = 0 V
–0.1 V
–0.2 V
IQE [%]
Wavelength [nm]

Fig. 1

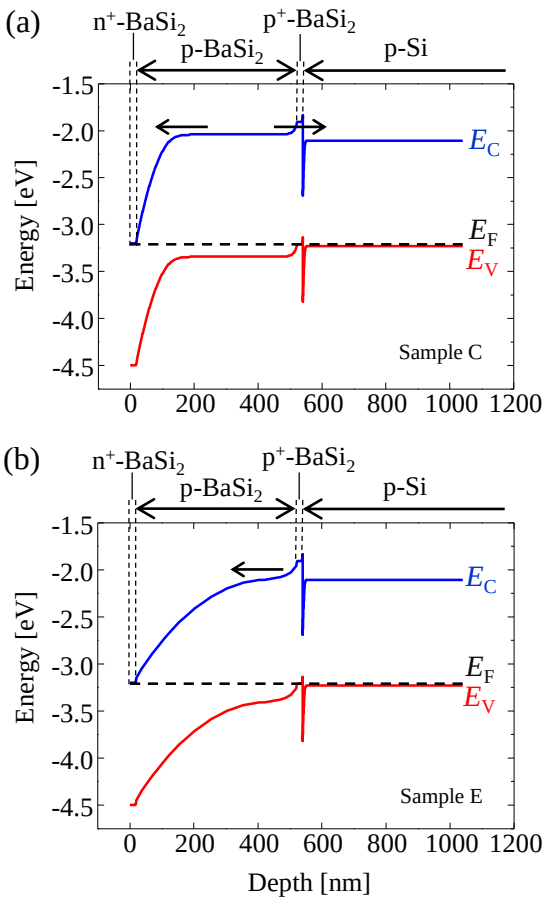
(a)
n+-BaSi2
p+-BaSi2
p-BaSi2
p-Si
-1.5
-2.0
-2.5
-3.0
-3.5
-4.0
-4.5
Energy [eV]
EC
EF
EV
Sample C
0
200
400
600
800
1000
1200
(b)
n+-BaSi2
p+-BaSi2
p-BaSi2
p-Si
Energy [eV]
EC
EF
EV
Sample E
Depth [nm]

Fig. 2

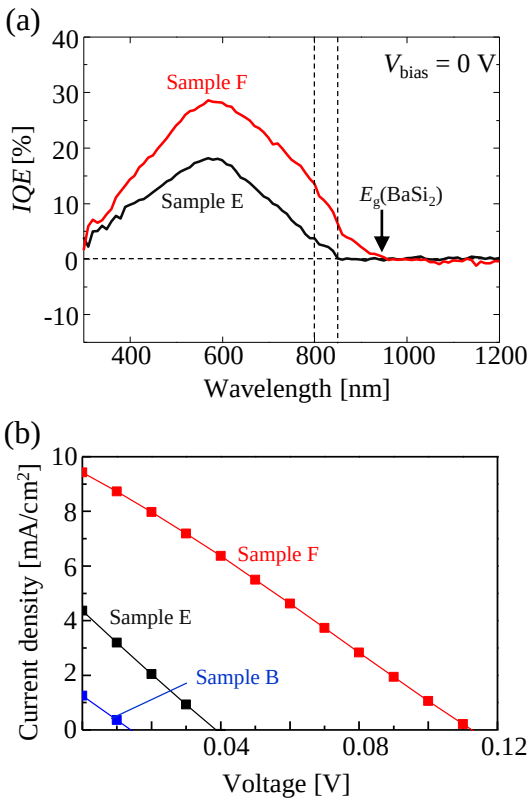
(a)
40
30
20
10
0
-10
IQE [%]
Sample F
Sample E
V_{bias} = 0 V
$E_g(BaSi_2)$
400
600
800
1000
1200
Wavelength [nm]
(b)
10
8
6
4
2
0
Current density [mA/cm^2]
Sample F
Sample E
Sample B
0.04
0.08
0.12
Voltage [V]

Fig. 3

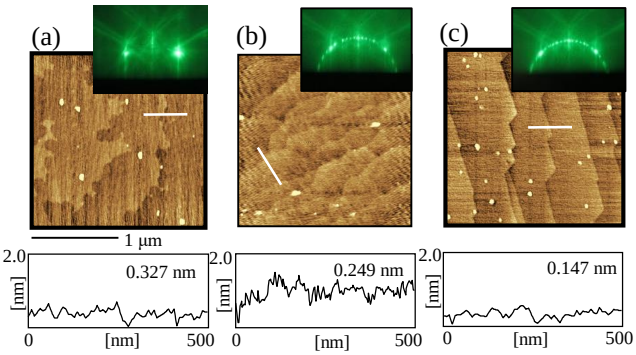
(a)
(b)
(c)
1 μm
2.0
0.327 nm
[nm]
0
[nm]
500
2.0
0.249 nm
[nm]
0
[nm]
500
2.0
0.147 nm
[nm]
0
[nm]
500

Fig. 4